

Dynamical effect of gas on spiral pattern speed in galaxies

Soumavo Ghosh^{1*}, and Chanda J. Jog^{1†}

¹ *Department of Physics, Indian Institute of Science, Bangalore 560012, India*

8 September 2021

ABSTRACT

In the density wave theory of spiral structure, the grand-design two-armed spiral pattern is taken to rotate rigidly in a galactic disc with a constant, definite pattern speed. The observational measurement of the pattern speed of the spiral arms, though difficult, has been achieved in a few galaxies such as NGC 6946, NGC 2997, and M 51 which we consider here. We examine whether the theoretical dispersion relation permits a real solution for wavenumber corresponding to a stable wave, for the observed rotation curve and the pattern speed values. We find that the disc when treated to consist of stars alone, as is usually done in literature, does not generally support a stable density wave for the observed pattern speed. Instead the inclusion of the low velocity dispersion component, namely, gas, is essential to obtain a stable density wave. Further, we obtain a theoretical range of allowed pattern speeds that correspond to a stable density wave at a certain radius, and check that for the three galaxies considered, the observed pattern speeds fall in the respective prescribed range. The inclusion of even a small amount ($\sim 15\%$) of gas by mass fraction in the galactic disc is shown to have a significant dynamical effect on the dispersion relation and hence on the pattern speed that is likely to be seen in a real, gas-rich spiral galaxy.

Key words: galaxies: kinematics and dynamics - galaxies: spiral - galaxies: structure - galaxies: Interstellar Medium - galaxies: individual: NGC 6946 - galaxies: individual: M 51

1 INTRODUCTION

Various surveys on galaxy morphology have revealed that the spiral structure is mainly of two types: flocculent structure, and grand-design spiral structure (Elmegreen et al. 2011). According to the density wave theory, the grand-design spiral pattern is a density wave that rotates rigidly in a galactic disc, and is maintained by the disc gravity (Lin & Shu 1964, 1966), also see Dobbs & Baba (2014) for a recent review.

The determination of pattern speed is of particular interest in galactic dynamics as it sets the location of resonance points where angular momentum transport is believed to occur, thus it has direct implications for the secular evolution of the galactic disc (Lynden-Bell & Kalnajs 1972). Over the years, several techniques have been devised to measure the pattern speed of these spiral structures. A common technique that is used is based on the assumed knowledge of the location of the resonance points (Buta & Combes 1996), which involves understanding the behaviour of stars and gas at these resonance points. Thus, estimation of the resonance

points from the observed surface brightness profiles, will give the value of pattern speed (Puerari & Dottori 1997). Another approach relies on information regarding the sign reversal of the radial streaming motion across the corotation. This can be done by studying a strip covering the kinematical minor-axis, where the radial component of the velocity has a non-zero projection along the line of sight. This method requires the position angle of the strip to be known accurately, which is not easy to check observationally because warps, often present in the outer parts of a galaxy, twist the location of the position angles. A related method, first proposed by Canzian (1993), employs the change of sign of radial streaming motion across corotation and also takes account of the geometric phase values. This technique has been applied successfully first to NGC 4321 (Sempere et al. 1995). Also, the pattern speed can be estimated from the observed azimuthal age-gradient of the young stellar complexes which are seen to be associated with the spiral arms (Grosbol & Patsis 1998). This technique has been applied to NGC 2997 to measure its pattern speed (Grosbol & Dottori 2009). Other popular method is the Tremaine-Weinberg method (hereafter, the TW method) which requires no specific dynamic model and predicts the value of pattern speed from kinematic measurements only (Tremaine & Weinberg

* E-mail : soumavo@physics.iisc.ernet.in

† E-mail : cjjog@physics.iisc.ernet.in

1984). In the past, the TW method has been used to deduce the pattern speed of bars (Merrifield & Kujiken 1995; Corsini, Debattista & Aguerri 2003; Maciejewski 2006) and spiral structures (Fathi et al. 2007). Each of the above methods involves different possible sources of errors or inaccuracies (see e.g. the discussion in Junqueira et al. 2015).

Spiral galaxies also contain a certain amount of interstellar gas whose fraction varies with their Hubble type (e.g. Young & Scoville 1991; Binney & Merrifield 1998). The role of gas has been studied in various contexts in galactic dynamics, and it has been shown that the low velocity dispersion component, namely, gas has a significant effect on stability against both local axisymmetric (Jog & Solomon 1984a,b; Bertin & Romeo 1988; Jog 1996; Rafikov 2001) and non-axisymmetric (Jog 1992) perturbations.

The longevity of a density wave was questioned by Toomre (1969) who showed that a wavepacket of density waves would propagate radially with a group velocity $c_g(R) = \partial\omega(k, R)/\partial k$, where ω and k are the frequency and the wavenumber, respectively, and R is the radius; and the dependence of ω on k is determined by the corresponding dispersion relation. This results in winding up of the wavepacket in a time-scale of about 10^9 years. A recent work by Ghosh & Jog (2015) showed that the inclusion of gas in the disc makes the group transport slower by a factor of few, thus allowing the pattern to persist for a longer time-scale. They also showed that for the observed pattern speed of $18 \text{ km s}^{-1} \text{ kpc}^{-1}$ (Siebert et al. 2012) and for assumed values of Toomre Q-parameters for our Galaxy, the disc when modelled as a stars-alone case, does not give a stable wave solution. Instead, one needs to invoke gas in order to get a stable density wave solution for the observed pattern speed.

In this paper, we study this in more detail and show this to be a general result: for this we study three external galaxies, NGC 6946, NGC 2997, and M 51 (NGC 5194) for which the observational values of the pattern speeds for the spiral structure and the rotation curves are available in the literature. We first treat the galactic disc as comprised only of stars and from the dispersion relation we obtain the lowest possible value of the dimensionless frequency (see § 2.2 for details) for which stars-alone will allow a stable wave. We next include gas on an equal footing with stars and follow the same procedure except for a two-component dispersion relation. We find that, at a radius equal to two disc scale-lengths and for an assumed set of Toomre Q parameter values, the stars-alone cases for NGC 6946 and NGC 2997 do not support a stable wave while for M 51, the stars-alone case marginally supports a stable density wave for the observed pattern speed. One has to include a gas fraction appropriate for the galaxies considered here, to get a stable density wave corresponding to the observed pattern speed. As a check, we also varied the parameters considered, covering a reasonable range of values, and confirmed the validity of this finding. Also, based on these calculations, we derive a range of allowed pattern speeds that yields a stable density wave at a given radius of a galaxy. We apply this method to these three galaxies, and find that the observed pattern speed values indeed fall in this prescribed range.

§ 2 describes the formulation of the problem while § 3 presents the results. § 4 and § 5 contain the discussion and conclusion, respectively.

2 FORMULATION OF THE PROBLEM

We treat the galactic disc as a gravitationally coupled two-component (star plus gas) system, where the stars are treated as a collisionless system and characterized by the surface density Σ_{0s} and the one-dimensional velocity dispersion σ_s . The gas is treated as a fluid, characterized by the surface density Σ_{0g} and a one-dimensional velocity dispersion or sound speed σ_g . Note that in any real galaxy, gas is seen to be present in both atomic (HI) and molecular (H_2) hydrogen form, having different surface density (Young & Scoville 1991; Bigiel & Blitz 2012) and velocity dispersion profiles (Tamburro et al. 2009). For the sake of simplicity, here we treat gas as a single-component and study its effect on the dispersion relation. The galactic disc is taken to be infinitesimally thin and the pressure acts only in the disc plane. In other words, we are interested in gravitational perturbations in the disc plane only. We use the cylindrical co-ordinates (R, ϕ, z).

2.1 Dispersion relation in the WKB limit

Consider the above system being perturbed by linear perturbations of the type $\exp[i(kr - \omega t)]$, where k is the wavenumber and ω is the frequency of the perturbation. For such a system, the dispersion relation in the WKB (Wentzel - Kramers - Brillouins) limit or the tightly wound case is (Ghosh & Jog 2015)

$$\frac{2\pi G \Sigma_{0s} |k| F\left(\frac{\omega - m\Omega}{\kappa}, \frac{k^2 \sigma_s^2}{\kappa^2}\right)}{\kappa^2 - (\omega - m\Omega)^2} + \frac{2\pi G \Sigma_{0g} |k|}{\kappa^2 - (\omega - m\Omega)^2 + \sigma_g^2 k^2} = 1 \quad (1)$$

where F is the reduction factor which physically takes into account the reduction in ω^2 arising due to the velocity dispersion of stars. The functional form of F is as given in Binney & Tremaine (1987). Here Ω is the angular frequency and κ is the local epicyclic frequency at a given radius.

After some algebraic simplifications (for details see Ghosh & Jog 2015), the dispersion relation (equation 1) reduces to

$$(\omega - m\Omega)^2 = \frac{1}{2} \{ (\alpha_s + \alpha_g) - [(\alpha_s + \alpha_g)^2 - 4(\alpha_s \alpha_g - \beta_s \beta_g)]^{1/2} \} \quad (2)$$

where,

$$\begin{aligned} \alpha_s &= \kappa^2 - 2\pi G \Sigma_{0s} |k| F\left(\frac{\omega - m\Omega}{\kappa}, \frac{k^2 \sigma_s^2}{\kappa^2}\right) \\ \alpha_g &= \kappa^2 - 2\pi G \Sigma_{0g} |k| + k^2 \sigma_g^2 \\ \beta_s &= 2\pi G \Sigma_{0s} |k| F\left(\frac{\omega - m\Omega}{\kappa}, \frac{k^2 \sigma_s^2}{\kappa^2}\right) \\ \beta_g &= 2\pi G \Sigma_{0g} |k| \end{aligned} \quad (3)$$

Now we define two dimensionless quantities, s , the dimensionless frequency and x , the dimensionless wavenumber as

$$s = (\omega - m\Omega)/\kappa = m(\Omega_p - \Omega)/\kappa, \quad x = k/k_{crit} \quad (4)$$

where $k_{crit} = \kappa^2/2\pi G(\Sigma_{0s} + \Sigma_{0g})$. Substituting equation (4)

in equation (2), we get the dimensionless form of the dispersion relation as (see equations (7) & (8) in Ghosh & Jog 2015):

$$s^2 = \frac{1}{2}[(\alpha'_s + \alpha'_g) - \{(\alpha'_s + \alpha'_g)^2 - 4(\alpha'_s\alpha'_g - \beta'_s\beta'_g)\}^{1/2}] \quad (5)$$

where,

$$\begin{aligned} \alpha'_s &= 1 - (1 - \epsilon)|x|F(s, \chi) \\ \alpha'_g &= 1 - \epsilon|x| + \frac{1}{4}Q_g^2\epsilon^2x^2 \\ \beta'_s &= (1 - \epsilon)|x|F(s, \chi) \\ \beta'_g &= \epsilon|x| \end{aligned} \quad (6)$$

and, $\chi = k^2\sigma_s^2/\kappa^2 = 0.286Q_s^2(1 - \epsilon)^2x^2$. The three dimensionless parameters Q_s , Q_g , and ϵ are respectively the Toomre Q factors for stars as a collisionless system ($Q_s = \kappa\sigma_s/(3.36G\Sigma_{0s})$), and for gas ($Q_g = (\kappa\sigma_g/(\pi G\Sigma_{0g}))$) (Toomre 1964), and $\epsilon = \Sigma_{0g}/(\Sigma_{0s} + \Sigma_{0g})$ is the gas mass fraction in the disc.

Similarly, the one-component analog of this dispersion relation is (Binney & Tremaine 1987):

$$s^2 = 1 - |x|F\left(\frac{\omega - m\Omega}{\kappa}, \frac{k^2\sigma_s^2}{\kappa^2}\right) \quad (7)$$

The dispersion relations (equation 7 for stars-alone and equation 5 for the two-component case) provide the information about how the dimensionless frequency s varies locally with respect to the dimensionless wavenumber x . Note that the equations (5) and (7) are symmetric with respect to both s and x , hence we consider only their absolute values throughout this paper. It is clear that the absolute value of s ($|s|$) ranges from 0 to 1, where $s = 0$ yields the position of corotation (hereafter CR) and $|s| = 1$ gives the positions of Lindblad resonances (Binney & Tremaine 1987).

It has been shown that for any $Q_s > 1$, there exists a zone between Lindblad resonance and corotation, known as the forbidden region where the dispersion relations (equations 5 and 7) have no real solution for $|k|$. Hence the corresponding density wave solutions, that fall in that range, will be evanescent, i.e. they will have complex wavenumber k , and they will either decay or grow exponentially (Binney & Tremaine 1987). A similar result holds when a two-component system has real $|s|$ solution.

A wavepacket, starting from the long-wave branch of the dispersion relation ($|x| < 1$), travels inward with a negative group velocity and gets reflected from the edge of the forbidden region near the CR, and then starts travelling radially outward in the short-wave branch ($|x| > 1$) with a positive group velocity (see Fig. 1) before finally being absorbed at a large wavenumber by a process similar to Landau damping (Binney & Tremaine 1987).

2.2 Method

Note that, in the density wave theory, the pattern speed of the grand-design two-armed spiral structure, Ω_p ($= \omega/m$; $m = 2$ here for spirals) is treated as a free parameter (e.g., Lin & Shu 1966), and its value is obtained from observations. Thus for a given observed value of Ω_p and from the observed rotation curve, the dimensionless frequency $|s|$

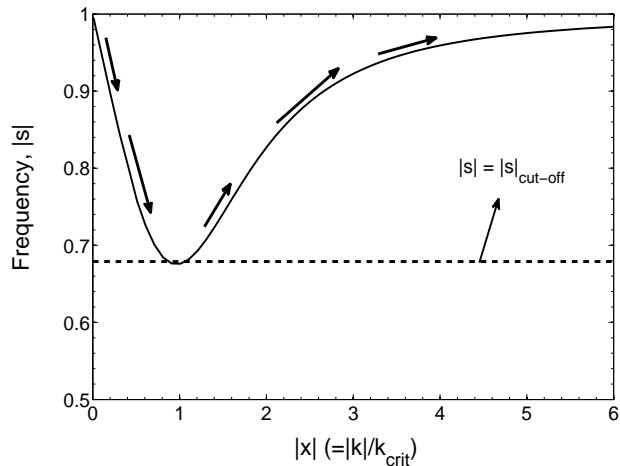


Figure 1. The dimensionless frequency $|s|$ vs. the dimensionless wavenumber $|x|$ from the dispersion relation for the stars-alone case (equation 7), plotted for $Q_s = 1.7$. Since the dispersion relation is symmetric in both s and x , only their absolute values are shown here. The arrows denote the direction of propagation of a typical density wavepacket. The horizontal line $|s| = |s|_{\text{cut-off}}$ indicates the lowest possible value of $|s|$, for which one can get a stable wave solution.

($= m|\Omega_p - \Omega|/\kappa$) (equation 4), has a definite value at a certain radius R , say $|s|_{\text{obs}}$. Therefore, for getting a stable density wave, the observationally found $|s|_{\text{obs}}$ value should fall in the allowed range of $|s|$, derived from the dispersion relation, both obtained at the same radius. In other words, the horizontal line $|s| = |s|_{\text{obs}}$ should cut the plot of $|s|$ versus $|x|$ at that radius, to yield a stable wave solution (i.e. a real solution for $|k|$), otherwise it will give an evanescent density wave solution.

We define $|s|_{\text{cut-off}}$ as the lowest possible value of $|s|$ for which one is able to get a stable wave solution from the dispersion relation at a given radius R . We set $|s|_{\text{cut-off}}$ as the lowest $|s|$ -value, where the plot of the dispersion relation turns around (equation (5) or equation (7), whichever is applicable). In other words, $|s|_{\text{cut-off}}$ indicates the edge of the forbidden region. A typical example of how $|s|_{\text{cut-off}}$ is obtained from a dispersion relation for a stars-alone case, is shown in Fig. 1. For the sake of illustration, we assume $Q_s = 1.7$, as observed in the solar neighbourhood (Binney & Tremaine 1987).

Thus, if the following inequality holds for a certain radius R :

$$|s|_{\text{obs}} \geq |s|_{\text{cut-off}} \quad (8)$$

then one can say that the observed pattern speed will give a stable density wave, and the dispersion relation will have real solution for $|k|$. Throughout this paper, $|s|_{\text{cut-off}}$ will be used for making quantitative statements regarding the existence of stable solutions.

3 RESULTS

3.1 Input parameters

We consider three galaxies for which the observational values for the input parameters, namely the pattern speed and the rotation curve, are available in the literature.

3.1.1 NGC 6946

This is a barred grand-design spiral galaxy with the Hubble type Scd. It has an angle of inclination 38° (Carignan et al. 1990; Boomsma 2007) and it is located at a distance of 5.5 Mpc (Kennicutt et al. 2003). The pattern speed of the main $m = 2$ gravitational perturbation i. e., the large oval and the two prominent spiral arms is measured to be 22^{+4}_{-1} km s $^{-1}$ kpc $^{-1}$ by Fathi et al. (2007), using the TW method. They also derived the locations of different resonance points (see table 2 there). The HI rotation curve is taken from Boomsma (2007). The exponential disc scale-length is measured as 1.9' or 3.3 kpc, where $1' = 1.75$ kpc (Carignan et al. 1990).

3.1.2 NGC 2997

This is a grand-design spiral galaxy of the Hubble type Sc (Milliard & Marcelin 1981). The pattern speed of the grand-design spiral structure is measured to be 16 km s $^{-1}$ kpc $^{-1}$ by Grosbol & Dottori (2009), by using the measurement of azimuthal age-gradient of newly formed stars. The rotation curve is taken from Peterson (1978). The exponential disc scale-length is measured as 4.0 kpc (Grosbol, Block, & Patsis 1999)

3.1.3 M 51 (NGC 5194)

This is a face-on spiral galaxy of the Hubble type Sc and is located at a distance of 9.6 Mpc (Sandage & Tammann 1975), in close interaction with NGC 5195. The pattern speed of the spiral structure is measured to be 38 km s $^{-1}$ kpc $^{-1}$ by Zimmer, Rand & McGraw (2004), using CO as a tracer and by applying the TW method. The rotation curve for M 51 is found to be steeply rising up to $\sim R = 25''$ and then for $R > 25''$ it saturates to 210 km s $^{-1}$ (Rand 1993), where $1'' = 46.5$ pc, assuming a distance of 9.6 Mpc (Sandage & Tammann 1975). The observed rotation curve and the observed pattern speed together place the CR at a distance of 5.5 kpc. The exponential disc scale-length is measured in various wavelengths and is found to vary from 4.36 kpc in B-band to 3.77 kpc in R-band (Beckman et al. 1996). We took a mean value of 4.0 kpc for the present purpose.

3.2 Stars-alone case

We first investigate whether a disc, consisting only of stars, can support a stable density wave for the observed values of pattern speed in different galaxies. To do this, first we obtained $|s|_{\text{obs}}$ at a radius of $2R_d$, R_d being the exponential disc scale-length, in each of these three galaxies. The choice of $2R_d$ is made because the spiral structure is typically seen in the middle part of an optical disc whose size is $\sim 4\text{-}5 R_d$ (e.g., Binney & Merrifield 1998). We found that the $|s|_{\text{obs}}$

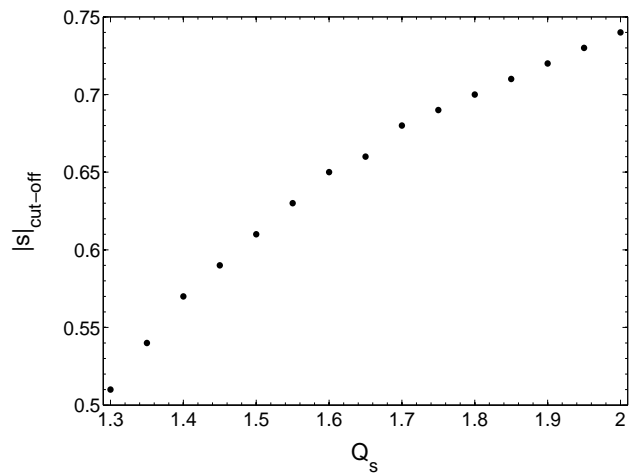


Figure 2. $|s|_{\text{cut-off}}$, the lowest values of the dimensionless frequency for which a stable density wave solution is possible, plotted as a function of Q_s , obtained from the one-component dispersion relation (equation 7). The resulting $|s|_{\text{cut-off}}$ value shows a steady increase with Q_s , thereby implying an increase in the forbidden region.

values for NGC 6946, NGC 2997, and M 51 are 0.38, 0.44, and 0.63 respectively.

Now to check whether the inequality given in equation (8) is satisfied or not, we need to calculate the $|s|_{\text{cut-off}}$ value from the dispersion relation (equation 7) for these galaxies. Note that the calculation of $|s|_{\text{cut-off}}$ from the dispersion relation requires the knowledge of Q_s , and the values of Q_s at different radii for a galaxy are not known observationally for most galaxies. We assume Q_s to be constant with R for simplicity, but in reality its values will vary (e.g., see Jog 2014; Ghosh & Jog 2014). Further, for a theoretical study, we varied the value of this radially-constant Q_s from 1.3 to 2.0, while 1.7 is the typical value in the solar neighbourhood (Binney & Tremaine 1987). The plot of the resulting $|s|_{\text{cut-off}}$ versus Q_s is shown in Fig. 2. From Fig. 2, we see that the $|s|_{\text{cut-off}}$ value increases steadily with the increase of Q_s , thereby implying a steady increase in the forbidden region around the CR as the Q_s value increases.

On comparing the $|s|_{\text{obs}}$ values that we obtained for both NGC 6946 and NGC 2997, with Fig. 2, we find that the inequality given by equation (8) is not satisfied for any value of Q_s , considered here. Thus, the dispersion relation for a purely stellar disc does not yield a real solution for $|k|$ and hence it does not yield a stable density wave corresponding to the observed pattern speeds of both these galaxies. For M 51, the stars-alone case barely supports a stable density wave when $Q_s = 1.5$, but if it is set to a value larger than 1.5, then the stars-alone case no longer supports a stable density wave for the observed pattern speed.

3.3 Stars plus gas case

We next include the interstellar gas, which has a low velocity dispersion as compared to the stars, in the system, and study whether the inclusion of gas helps in getting a stable wave solution for the observed pattern speeds. First we investigated how the values of $|s|_{\text{cut-off}}$ change with different

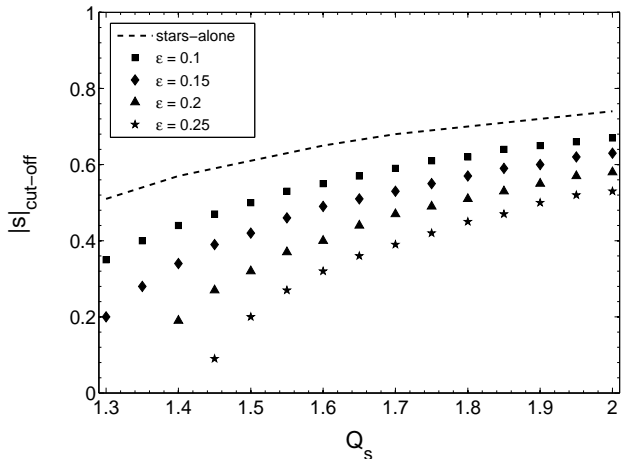


Figure 3. $|s|_{\text{cut-off}}$, the lowest values of the dimensionless frequency for which a stable density wave solution is possible for the two-component case, plotted as a function of Q_s , for different gas fractions (ϵ) and $Q_g = 1.5$. The labels used for different gas fractions are as indicated in the legend. With increasing gas fraction, the $|s|_{\text{cut-off}}$ decreases steadily for the whole range of Q_s considered here. Thus the extent of the forbidden region decreases with increasing gas fraction.

values for the three parameters Q_s , Q_g , and ϵ . We varied Q_s from 1.3 to 2.0 and ϵ from 0.1 to 0.25. In each case we fix Q_g , and then compute $|s|_{\text{cut-off}}$ from equation (5), as a function of Q_s , and repeat this procedure for different values of ϵ . For comparison, we replotted the $|s|_{\text{cut-off}}$ values for the stars-alone case, as a function of Q_s . The result for $Q_g = 1.5$ is shown in Fig. 3. From Fig 3, it is clear that with the inclusion of more gas (i.e., higher ϵ value), the $|s|_{\text{cut-off}}$ value steadily decreases. This holds true for the above mentioned range of Q_s values, at a given Q_g . In other words, a larger value of gas fraction (ϵ) helps to decrease the forbidden region around the CR, and thus allowing a higher range of permitted pattern speeds (for details see § 3.4). For the other values of Q_g in the range of 1.4 to 1.8, we got a similar trend, hence we do not produce them here.

Now we investigate the dynamical effect of gas on the grand-design spiral structure for the three specific galaxies, chosen for this work. The value of $|s|_{\text{cut-off}}$ is obtained from the dispersion relation for a two-component system (equation 5) for a set of values for the three dimensionless input parameters (Q_s , Q_g , ϵ). The values used are $Q_s = 1.5$ and $Q_g = 1.5$ for the stars plus gas case, and $Q_s = 1.5$ for the stars-alone case, with $\epsilon = 0.25$ for NGC 6946 and $\epsilon = 0.15$ for NGC 2997 and M 51, as typical for their Hubble types (see fig. 5, Young & Scoville 1991). Then we checked whether or not the value of $|s|_{\text{cut-off}}$ obtained theoretically from the dispersion relation for the above input parameters, and the value of $|s|_{\text{obs}}$ obtained from observations satisfy the inequality in equation (8). The results for NGC 6946, NGC 2997, and M 51 are shown in Fig. 4, Fig. 5, and in Fig. 6, respectively.

Since, the above values of Q_s and Q_g are chosen in a somewhat ad-hoc way, hence for each galaxy, we next study the variation in the dispersion relation for a reasonable range of Q_s and Q_g values, $Q_s = 1.5, 1.6, 1.7$ and $Q_g = 1.4, 1.5, 1.6$ and 1.7 . The typical gas fraction value, chosen as per

the Hubble type of any individual galaxy (for details see Young & Scoville 1991) is kept constant. We found that, for a fixed ϵ , there is a strong variation in the behaviour of the dispersion relation for different Q_s values, as compared to the different Q_g values. A higher gas fraction (ϵ) would be expected to change the results substantially, as suggested by Jog & Solomon (1984a, see fig. 3 there), but here we have kept ϵ constant as typical for a given Hubble type.

Fig. 4, and Fig. 6 show that for NGC 6946 and M 51, the $|s|_{\text{obs}}$ value lies above the $|s|_{\text{cut-off}}$ value for the star-gas system, thus the inequality given by equation (8) is satisfied, and this is true for the whole range of parameter space considered here. Thus the stars plus gas case allows a stable solution. For NGC 2997, the inequality given by equation (8) is satisfied only for $Q_s = 1.5$. For a Q_s value higher than 1.5, even the addition of gas in the two-component system no longer admits a stable density wave (see Fig. 5). In contrast, for $Q_s < 1.5$, the two component system admits a stable density wave solution. This can be seen from the result that as Q_s decreases, the $|s|_{\text{cut-off}}$ for the stars plus gas also decreases, so that the forbidden region is smaller (see Fig. 3).

Hence, the galactic disc when treated as a gravitationally coupled stars plus gas system, with the observed gas fraction, allows a stable wave solution for the observed pattern speed, for most of the parameter range considered here. This is the main finding from this paper.

Interestingly, we see that for both NGC 6946 and NGC 2997 (Fig. 4 & Fig. 5 (a)), the observed value of $|s|_{\text{obs}}$ is close to the $|s|_{\text{cut-off}}$ value which is obtained theoretically from the dispersion relation for the stars plus gas case (equation 5), but not the $|s|_{\text{cut-off}}$ value obtained for the stars-alone case (equation 7). Note that the curve for the dispersion relation for stars-alone case lies above that for the stars plus gas case, so if the pattern speed were such that the corresponding observed $|s|_{\text{obs}}$ were to be greater than the cut-off value for the stars-alone case it would also be greater than the cut-off value for the two-component case. Thus if a pattern speed value gives a stable density wave solution for a one-component case, it will also give so for the two-component case. Also the observed value of $|s|_{\text{obs}}$ lies close to the two-component $|s|_{\text{cut-off}}$ value (but see M 51), and this means that a galaxy seems to “prefer” to have a pattern speed that is indicated by the stars-plus-gas case for the observed gas fraction.

This can be explained as follows. A joint two-component system is more unstable to the growth of perturbations or is closer to being unstable than the stars-alone case (Jog & Solomon 1984), and this results in a lower cut-off $|s|_{\text{cut-off}}$ for the two component case than the stars-alone case. If the galactic disc were subjected to perturbations having a range of values for pattern speeds (say as arising due to a tidal interaction), then the perturbation most likely to be amplified in a galaxy is the one for which the dimensionless frequency $|s|_{\text{cut-off}}$ has the lowest value, as this would correspond to the fastest growing perturbation.

This indicates that the inclusion of even 15 to 25 per cent gas fraction by mass has a non-trivial effect on the determination of the pattern speed that a galaxy is likely to have. The value of the pattern speed, along with the rotation curve, sets the locations of the Lindblad resonances in the disc. These are important in determining the secular

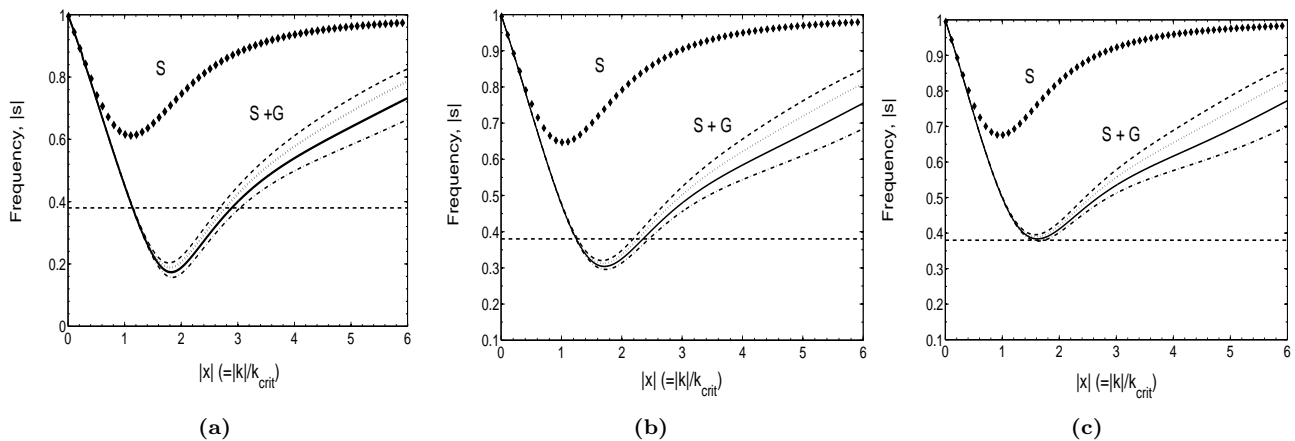


Figure 4. *NGC 6946*: Dispersion relations for stars-alone (S) and stars plus gas (S + G) cases, plotted in a dimensionless form, for a range of Q_s and Q_g values, at $R = 2R_d$. Panel (a) for $Q_s = 1.5$, panel (b) for $Q_s = 1.6$, and panel (c) for $Q_s = 1.7$. In each panel, Q_g is taken to be 1.4, 1.5, 1.6, and 1.7, successively. The corresponding dispersion relations are shown from bottom to top. The horizontal line indicates the value $|s|_{\text{obs}}$, derived from the observed pattern speed and the rotation curve. Here in all the cases, the two-component case allows a real solution for $|k|$ and thus a stable density wave solution for the observed value of the pattern speed, but this is not true for the stars-alone case.

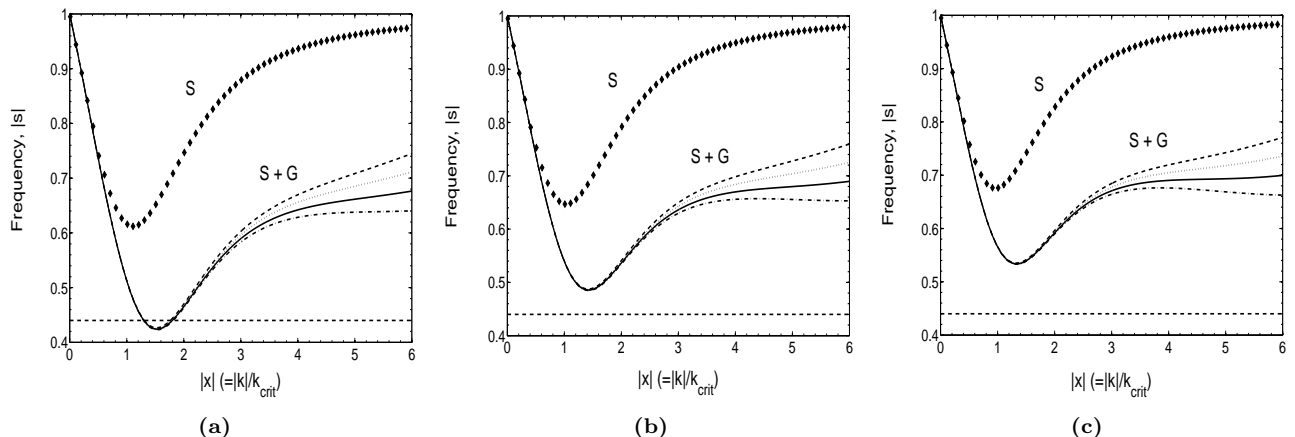


Figure 5. *NGC 2997*: Dispersion relations for stars-alone (S) and stars plus gas (S + G) cases, plotted in a dimensionless form, for a range of Q_s and Q_g values, at $R = 2R_d$. Panel (a) for $Q_s = 1.5$, panel (b) for $Q_s = 1.6$, and panel (c) for $Q_s = 1.7$. In each panel, Q_g is taken to be 1.4, 1.5, 1.6, and 1.7, successively. The corresponding dispersion relations are shown from bottom to top. The horizontal line indicates the value $|s|_{\text{obs}}$, derived from the observed pattern speed and the rotation curve. Here for $Q_s = 1.5$, the two-component case, but not the stars-alone case, allows a stable density wave solution while for other values of Q_s , none of the stars-alone and two-component case allows a stable density wave for the observed value of the pattern speed.

evolution of galactic disc via angular momentum transport (Lynden-Bell & Kalnajs 1972). Thus our work shows that the gas is important in setting the observed pattern speed in a galaxy and hence it is likely to play a crucial role in future dynamical evolution of a galactic disc.

We caution that the assumption of tight-winding (or, WKB limit), which played the crucial role in deriving the dispersion relations in equation (5) and equation (7), is suspect for the long-wave branch ($|x| < 1$). This is important especially for *NGC 2997*, where the real solution ($|x|$), i.e., where the line $|s| = |s|_{\text{obs}}$ cuts the dispersion relation, is less than 2 (see Fig. 5). To verify the validity of the tight-winding limit in a more quantitative manner for all three galaxies considered here, we calculated the quantity X , at a radius R equals to $2R_d$, where X is defined as follows:

$$X = \frac{\kappa^2 R}{2\pi G m \Sigma_{\text{tot}}} \quad (9)$$

Σ_{tot} denotes the sum of the surface densities of the stellar and the gaseous components and m ($= 2$, here) denotes the number of spiral arms. For the gas surface density tending to zero, it reduces to the usual X , defined for the one-component stellar case, as expected (for details see Binney & Tremaine 1987). The quantity X denotes the cotangent of the pitch angle of waves of the critical wavenumber k_{crit} and $X \gg 1$ implies that the spiral arm is tightly wound, and hence the tight-winding approximation holds good (Binney & Tremaine 1987). We followed the following prescription for calculating the quantity X . For a given gas fraction ϵ and for an observed gas sur-

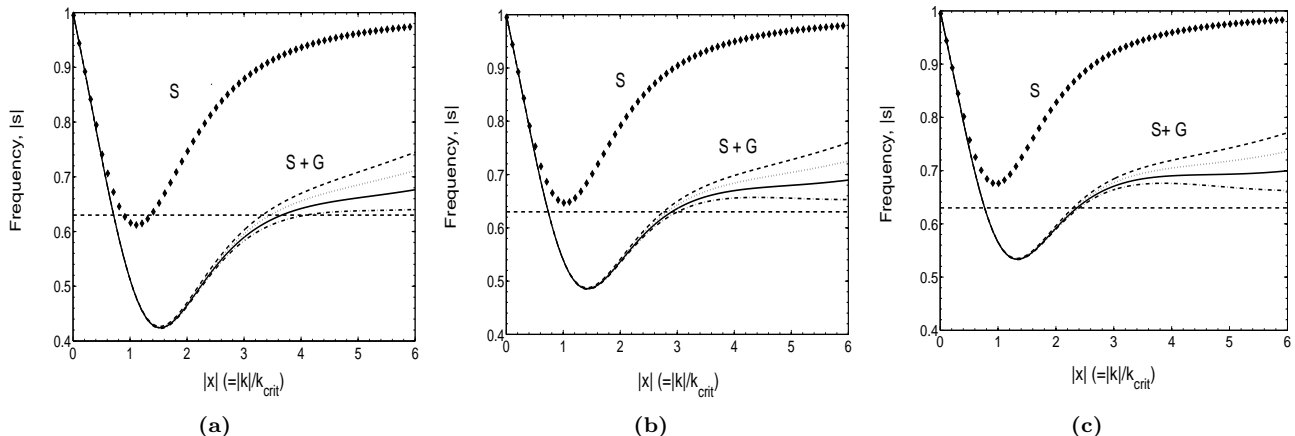


Figure 6. *M 51*: Dispersion relations for stars-alone (S) and stars plus gas (S + G) cases, plotted in a dimensionless form, for a range of Q_s and Q_g values, at $R = 2R_d$. Panel (a) for $Q_s = 1.5$, panel (b) for $Q_s = 1.6$, and panel (c) for $Q_s = 1.7$. In each panel, Q_g is taken to be 1.4, 1.5, 1.6, and 1.7, successively. The corresponding dispersion relations are shown from bottom to top. The horizontal line indicates the value $|s|_{\text{obs}}$, derived from the observed pattern speed and the rotation curve. Here for $Q_s = 1.5$, both the two-component case and the stars-alone case, allow a stable density wave solution, but for larger values of Q_s , only the two-component case allows a stable density wave for the observed value of pattern speed.

Table 1. Values for X for three galaxies, calculated at $R = 2R_d$

Galaxy name	R (kpc)	κ ($\text{km s}^{-1} \text{ kpc}^{-1}$)	Σ_g ($M_\odot \text{ pc}^{-2}$)	ϵ	Σ_{tot} ($M_\odot \text{ pc}^{-2}$)	X
NGC 6946	6.6	42.4	22.4	0.25	89.6	2.3
NGC 2997	8.0	32.7	8.3	0.15	55.3	2.7
M 51	8.0	37.1	10	0.15	66.7	2.9

face density at a given radius R , we can obtain the total surface density at that radius. Further from the observed rotation curve, the epicyclic frequency κ at $R = 2R_d$ is obtained. The total gas surface density for NGC 6946 is taken from Crosthwaite & Turner (2007) and for M 51, it is taken from Schuster et al. (2007). A similar distribution of the total gas surface density for NGC 2997, as a function of radius, is not available in the literature, to the best of our knowledge. So for this case we used the following technique to have an estimate of gas surface density. The HI observations for NGC 2997 give a total HI mass of $4.2 \times 10^9 M_\odot$, which extends over an area having mean diameter of 31.2 kpc (Kodilkar, Kantharia & Ananthkrishnan 2011). This, in turn, gives a mean HI surface density of $5.5 M_\odot \text{ pc}^{-2}$ for NGC 2997. Now assuming a constant value of 0.5 for the ratio of mass in HI to mass in H_2 (for details see Young & Scoville 1991), we get the mean surface density of H_2 . Then using ϵ , we get the total mean surface density which is used in equation (9) to derive the quantity X . The results for value of X for the three galaxies are given in Table 1. From Table 1, we see that the values of X is greater than 1, thus the tight-winding approximation is satisfied, though not by a comfortable margin.

3.4 A general constraint on pattern speeds

For a collisionless disc, the density wave can exist only in the regions where

$$\Omega - \kappa/2 \leq \Omega_p \leq \Omega + \kappa/2 \quad (10)$$

holds, and the equality holds only at the resonance points. Here in this section, we use our technique based on the calculation of $|s|_{\text{cut-off}}$ to constrain the range of allowed pattern speed for the $m = 2$, grand-design spiral structures, which will give a stable density wave. The prescription is as follows.

First we consider Q_s values in the range from 1.3 to 2.0 and Q_g also in the range from 1.4 to 1.8. The gas-fraction, ϵ , is varied from 5 to 25 per cent of the total disc mass, depending on the Hubble-type of a particular galaxy. Then for a fixed value of ϵ , we obtained the value of $|s|_{\text{cut-off}}$ for the whole range of Q_s and Q_g considered here. We found that for the gas-fraction of 5 per cent, the gas does not contribute much towards getting a stable density wave, but as the gas-fraction increases steadily, the effect of gas becomes more prominent. However, galaxies having $\epsilon > 25$ per cent mainly show a flocculent spiral structure and do not generally host a grand-design spiral structure (Elmegreen et al. 2011). Considering the above points, we have restricted the value of ϵ from 10 to 25 per cent.

Now suppose, at a certain radius R for a particular galaxy, one knows the value of ϵ , and one can make a reasonable choice for the values of Q_s and Q_g . Then from these parameters, we can obtain the value of $|s|_{\text{cut-off}}$, call it α . Then, to get a stable wave, the pattern speed (Ω_p) has to satisfy equation (8) with $|s|_{\text{obs}}$ being replaced by $|s|$. This in turn gives

$$s \geq \alpha \quad \text{or} \quad s \leq -\alpha \quad (11)$$

i.e.,

$$\Omega_p \geq \Omega + \frac{\alpha\kappa}{2} \quad \text{or} \quad \Omega_p \leq \Omega - \frac{\alpha\kappa}{2} \quad (12)$$

depending upon whether one is outside the CR or inside the CR. Now combining inequality (10) and (12), we can say

Table 3. Ranges of Q_s and Q_g for three galaxies, that give a stable wave solution

Galaxy name	ϵ	$R(= 2R_d)$ (kpc)	Range in Q_s	Range in Q_g
NGC 6946	0.25	6.6	1.3 - 1.7	1.4 - 1.8
NGC 2997	0.15	8.0	1.3 - 1.5	1.4 - 1.8
M 51	0.15	8.0	1.3 - 1.9	1.4 - 1.8

that when one is inside the CR then the allowed range of pattern speed would be $(\Omega - \kappa/2, \Omega - \alpha\kappa/2)$ and when one is outside the CR then the allowed range would be $(\Omega + \alpha\kappa/2, \Omega + \kappa/2)$.

We applied this technique to the three galaxies considered here, at $R = 2R_d$, using $Q_s = 1.5$ and $Q_g = 1.5$ that were used as a set of parameters in Fig. 4, Fig. 5 and Fig. 6. For NGC 6946 and NGC 2997, $R = 2R_d$ lies inside the CR, and for M 51, $R = 2R_d$ lies outside the CR. Hence following the above prescription, the predicted range of allowed pattern speeds that give a stable density wave, would be $(\Omega - \kappa/2, \Omega - \alpha\kappa/2)$ for NGC 6946 and NGC 2997, and for M 51, predicted range of allowed pattern speeds would be $(\Omega + \alpha\kappa/2, \Omega + \kappa/2)$. The results are summarized in Table 2. We check that the observed values of the pattern speed, 22 km s⁻¹ kpc⁻¹ for NGC 6946, 16 km s⁻¹ kpc⁻¹ for NGC 2997, and 38 km s⁻¹ kpc⁻¹ for M 51, do indeed lie within the respective range of allowed pattern speeds obtained theoretically.

We then varied Q_s from 1.3 to 2.0 and Q_g from 1.4 to 1.8 to see what ranges of these two parameter will allow the observed pattern speed of three galaxies, to fall in the range, predicted from our theoretical work, and thus give a stable density wave solution. These are summarized in Table 3.

We note that a lower value of Q_s or Q_g than their respective minima chosen here will give an even smaller forbidden region, hence the observed pattern speed would be also permitted for $Q_s < 1.3$ and $Q_g < 1.4$.

It is interesting to note that for NGC 6946, the allowed range for the pattern speed for a stable wave is obtained to be 8.8-17.1 km s⁻¹ kpc⁻¹ for stars-alone case, while the observed pattern speed 22 km s⁻¹ kpc⁻¹ clearly lies outside this allowed range. Similarly, for NGC 2997, the allowed range for the stars-alone case is calculated to be 6.8-13.5 km⁻¹ kpc⁻¹, while again the observed pattern speed 16 km s⁻¹ kpc⁻¹ lies outside this permitted range. Thus real galaxies seem to have pattern speed values that lie beyond the values required for a stable solution for the stars-alone case. The presence of gas pushes the galaxy to adopt a pattern speed which is higher than the stars-alone case. Thus the inclusion of gas will have effect in setting the pattern speed and thus in turn will effect the secular evolution of the disc galaxy (see § 3.3).

We also illustrate the effect of gas on pattern speeds in another way. Suppose we were to artificially decrease the gas fraction in NGC 6946 to be 15 per cent, then the allowed range for the pattern speeds is obtained to be 8.8-20.8 km⁻¹ kpc⁻¹ - this does not cover the observed pattern speed of 22 km s⁻¹ kpc⁻¹. Thus the actual value of gas mass fraction (ϵ) also matters in setting the value of pattern speed. The real galaxies studied seem to have pattern speeds that are close to the upper value in the allowed range, or in other words

when $|s|_{\text{obs}}$ is just higher than $|s|_{\text{cut-off}}$ (see the discussion in Section 3.3).

4 DISCUSSION

Here we mention a few points regarding this current work. First, the shape of the dispersion relation and hence the value of $|s|_{\text{cut-off}}$ is largely dependent on the values of the parameters (Q_s, Q_g, ϵ) chosen. Note that, for most of the galaxies, the observed radial profiles for Q_s and Q_g are not available. Consequently, one has to rely on educative guesses for these two Q-values, as we have done here. If the actual observed values for Q_s and Q_g are known, the findings of this paper can be put in a more accurate way.

Secondly, the density wave corresponding to the observed pattern speed may not be long lasting. In fact, some of the past N -body simulations of spiral galaxies have showed that the spiral arms fade out quickly in time (Dobbs & Baba 2014). However when a stellar disc is represented with sufficiently higher number of particles (\sim order of 10^8), the spiral structure in the simulations lasts for a time-scale of about a Hubble time, because in these cases the Poisson noise of the system is minimized (Fuji et al. 2011; D’Onghia, Vogelsberger, & Hernquist 2013). But, in general, N -body simulations of spiral galaxies show that an individual spiral arm is transient and gets wound up, which is at odds with a classical long-lived quasi-stationary density wave scenario (Sellwood 2011; Grand, Kawata, & Cropper 2012; Baba, Saitoh, & Wada 2013). The spiral structures could be more complex, for example, there is evidence that some galaxies could show either a long-lived spiral pattern or a short-lived pattern, or a galaxy could exhibit both types of patterns, e.g., see the discussion in Siebert et al. (2012).

Thirdly, all the results presented in this work, are based on the assumption of the existence of a quasi-stationary density wave that rotates in the galactic disc with a constant pattern speed. However, observational studies by Foyle et al. (2011) for a sample of 12 nearby late-type star-forming galaxies and by Ferreras et al. (2012) for NGC 4321 did not find any angular off-set in age as predicted by the classical density wave theory. This shows that the density wave theory does not seem to be applicable for these galaxies.

Finally, note that, the results presented here are based on a local calculation, whereas the density wave extends over a large range of radii in the galactic disc. The results indicate that gas may have a significant effect on the spiral arms for the large-scale as well. A global modal analysis for a gravitationally coupled two-component (star plus gas) galactic disc to study the effect of the gas on large-scale spiral arms will be taken up in a future study.

5 CONCLUSION

In summary, we have shown that the inclusion of gas is essential to get a stable density wave solution corresponding to the observed pattern speed in a spiral galaxy. We use a two-component (stars plus gas) dispersion relation for a galactic disc, and assume reasonable gas fraction and Toomre Q values for stars and gas. Then we check whether the theoretical dispersion relation permits a real $|k|$ solution (or a

Table 2. Range of allowed pattern speeds for NGC 6946, NGC 2997 & M 51 at $R = 2R_d$

Galaxy name	Ω (km s^{-1} kpc^{-1})	κ (km s^{-1} kpc^{-1})	ϵ (gas fraction)	observed Ω_p (km s^{-1} kpc^{-1})	α	Lower bound on Ω_p (km s^{-1} kpc^{-1})	Upper bound on Ω_p (km s^{-1} kpc^{-1})
NGC 6946	30.0	42.4	0.25	22	0.17	8.8	26.4
NGC 2997	23.1	32.7	0.15	16	0.42	6.8	16.2
M 51	26.2	37.1	0.15	38	0.42	34.0	44.8

stable wave) for the observed rotation curve and the pattern speed. Three galaxies of different Hubble type, NGC 6946, NGC 2997, and M 51, are chosen for which the pattern speed values of the grand-design spiral structure and the rotation curves are known from observations. We show that for both NGC 6946 and NGC 2997, at a radius of two disc scale-lengths, the stars-alone case is not able to produce a stable density wave corresponding to the observed pattern speeds, while for M 51, stars-alone case barely supports a stable density wave. One has to include the observed gas fraction in the study, in order to get a stable density wave for these pattern speeds. This is the main result from this work. Since these galaxies are typical representatives of their Hubble type, we expect that this finding will hold true for other grand-design spiral galaxies as well.

Based on the technique used here, we obtain a theoretical range of allowed pattern speeds that give a stable density wave at a certain radius of a galaxy. We apply this technique to the three galaxies considered here, and find that the observed pattern speeds of these three galaxies indeed fall in the respective prescribed range.

We show that the inclusion of even 15 to 25 per cent gas by mass fraction has a significant dynamical effect on the dispersion relation and hence on the pattern speed which is likely to be seen in a real, gas-rich galaxy. The resulting allowed range of pattern speeds is higher in presence of gas. The value of pattern speed affects the angular momentum transport. Thus, the gas is likely to play a crucial role in the secular evolution of a galaxy. The effect of gas on the large-scale spiral structure will be investigated in a future study.

Acknowledgements: We thank the anonymous referee for the constructive comments which have greatly helped to improve the paper. C.J. would like to thank the DST, Government of India for support via J.C. Bose fellowship (SB/S2/JCB-31/2014).

REFERENCES

- Baba J., Saitoh T. R., Wada K., G., 2013, *ApJ*, 763, 46
 Bertin G., Romeo A. B., 1988, *A&A*, 195, 105
 Beckman J. E., Peletier R. F., Knapen J. H., Corradi R. L. M., Gentet L. J., 1996, *ApJ*, 467, 175
 Bigiel F., Blitz L., 2012, *ApJ*, 756, 183
 Binney J., Merrifield M., 1998, *galactic Astronomy*. Princeton Univ. Press, Princeton, NJ
 Binney J., Tremaine S., 1987, *Galactic Dynamics*. Princeton Univ. Press, Princeton, NJ
 Boomsma R., 2007, Ph.D. thesis, Univ. Groningen
 Buta R., Combes F., 1996, *Fundam. Cosmic Phys.*, 17, 95
 Canzian B., 1993, *ApJ*, 414, 487
 Carignan C., Charbonneau P., Boulanger F., Viallefond F., 1990, *A&A*, 234, 43
 Crosthwaite L. P., Turner J. L., 2007, *ApJ*, 134, 1827
 Corsini E. M., Debattista V., Aguerri A., 2003, *ApJ*, 599, L29
 Dobbs C., Baba J., 2014, *PASA*, 31, 35
 D’Onghia E., Vogelsberger, M., Hernquist L., 2013, *ApJ*, 766, 34
 Elmegreen D. M. et al., 2011, *ApJ*, 737, 32
 Ferreras I., Cropper M., Kawata D., Page M., Hoversten E. A., 2012, *MNRAS*, 424, 1636
 Foyle K., Rix H. W., Dobbs C. L., Leroy A. K., Walter F., 2011, *ApJ*, 735, 101
 Fathi K., Toonen S., Falcon-Barroso J., Beckman J. E., Hernandez O., Daigle O., Carignan C., de Zeeuw T., 2007, *ApJ*, 667, L137
 Fuji M. S., Baba J., Saitoh T. R., Makino J., Kokubo E., Wada K., 2011, *ApJ*, 730, 109
 Ghosh S., Jog C. J., 2015, *MNRAS*, 451, 1350
 Ghosh S., Jog C. J., 2014, *MNRAS*, 439, 929
 Grand R. J. J., Kawata D., Cropper M., 2012, *MNRAS*, 426, 167
 Grosbol P., Dottori H., 2009, *A&A*, 499L, 21G
 Grosbol P., Block, D. L., Patsis, P. A., 1999, *Ap&SS*, 269, 423
 Grosbol P., Patsis P. A., 1998, *A&A*, 336, 840
 Jog C. J., 2014, *AJ*, 147, 132
 Jog C. J., 1996, *MNRAS*, 278, 209
 Jog C.J., 1992, *ApJ*, 390, 378
 Jog C.J., Solomon P.M., 1984 a, *ApJ*, 276, 114
 Jog C.J., Solomon P.M., 1984 b, *ApJ*, 276, 127
 Junqueira T. C., Chiappini C., Lepine J. R. D., Minchev I., Santiago, B. X., 2015, *MNRAS*, 449, 2336
 Kennicutt R. C. et al., 2003, *PASP*, 115, 928
 Kodilkar J., Kantharia N. G., Ananthkrishnan S., 2011, *MNRAS*, 416, 522
 Lin C. C., Shu F. H., 1966, *PNAS*, 55, 229
 Lin C. C., Shu F. H., 1964, *ApJ*, 140, 646
 Lynden-Bell D., Kalnajs A. J., 1972, *MNRAS*, 157, 1L
 Maciejewski W., 2006, *MNRAS*, 371, 451
 Merrifield M. R., Kuijken K., 1995, *MNRAS*, 274, 933
 Milliard B., Marcelin M., 1981, *A&A*, 95, 59
 Peterson C. J., 1978, *ApJ*, 226, 75
 Puerari I., Dottori H., 1997, *ApJ*, 476, L73
 Rafikov R. R., 2001, *MNRAS*, 323, 445
 Rand J. R., 1993, *ApJ*, 410, 68
 Sandage A., Tammann G. A., 1975, *ApJ*, 196, 313
 Schuster K. F., Kramer C., Hirschfeld M., Garcia-Burillo S., Mookerjee B., 2007, *A&A*, 461, 143

- Sempere M. J., Garcia-Burillo S., Combes F., Knapen J. H., 1995, *A&A*, 296, 45
Sellwood J. A., 2011, *MNRAS*, 410, 1637
Siebert A. et al., 2012, *MNRAS*, 425, 2335
Tamburro D., Rix H. W., Leroy A. K., Mac Low M. M., Walter F., Kennicutt R. C., Brinks E., de Blok W. J. G., 2009, *AJ*, 137, 4424
Toomre A., 1969, *ApJ*, 158, 899
Toomre A., 1964, *ApJ*, 139, 1217
Tremaine S., Weinberg M. D., 1984, *ApJ*, 282, L5
Young J. S., Scoville N. Z., 1991, *ARAA*, 29, 581
Zimmer P., Rand R. J., McGraw J. T., 2004, *ApJ*, 607, 285